ELSEVIER

Journal of Nuclear Materials 290–293 (2001) 990–994

journal of nuclear materials

www.elsevier.nl/locate/jnucmat

Non-axisymmetric perturbation of the plasma surface in RFX: analysis of magnetic data versus CCD images of plasma–wall interaction

P. Zanca *, D. Bettella, S. Martini, M. Valisa

Consorzio RFX CNR, Corso Stati Uniti 4, 35127 Padova, Italy

Abstract

In the RFX experiment, as in other reversed field pinches, the sustainment of the configuration in standard conditions entails the presence of a relatively wide spectrum of internally resonant tearing modes with saturated amplitude. Such modes cause a non-axisymmetric perturbation of the magnetic configuration. In this paper a detailed comparison of the perturbed magnetic surface with the footprint of enhanced plasma wall interaction evidenced by CCD camera images of the RFX graphite first wall is presented. The comparison confirms the accuracy of the magnetic reconstruction algorithm, which computes peak-to peak perturbation of the plasma surface as large as 5 cm in some cases and a contribution from $m = 0$ modes which can be comparable to that of $m = 1$ modes, particularly at low currents.

Keywords: RFX

1. Introduction

The sustainment of a reversed field pinch (RFP) magnetic configuration entails a dynamo mechanism, which is produced by a spectrum of $m = 0, 1$, internally resonant resistive tearing modes [1]. These modes have a natural tendency to lock in phase between themselves [2] and in the RFX device ($R = 2$ m, $a = 0.457$ m, $I \leqslant 2$ MA) [3] they also always lock to the wall. This phenomenon causes a stationary non-axisymmetric perturbation of the magnetic surfaces (dubbed locked mode or LM), resulting in toroidally localised helical paths of strongly enhanced plasma wall interaction (PWI). Such localised PWI zones are characterised by intense emission in the visible range due to the influx of hydrogen and impurities (mainly carbon) atoms emitted from the strongly heated graphite tiles which covers entirely the RFX vacuum vessel.

In this paper we present a detailed cross-correlated analysis of the magnetic perturbation and of the evidence of localised enhanced PWI. The magnetic configuration is computed by a non-axisymmetric reconstruction method [4,5] using the measurements of arrays of local B_ϕ pick-up coils. The paths where the localised enhanced PWI occurs are identified by analysing the images of CCD cameras.

2. CCD camera images

A detailed description of the RFX viewing system is given in [6]. The CCD cameras used to monitor the plasma–wall interaction are commercial devices with 25 frame/s of time resolution and about 50 dB of dynamic range. Spatial resolution is excellent for the purpose with about 768×576 pixels. The digital acquisition is synchronised with the experiment. Typically, the observations are carried out in the C II light, that is by interposing an interference filter centred around 515.5 ± 2.5 nm, which makes the observation sensitive to the carbon influx. Spectroscopic analysis, based on

* Corresponding author. Tel.: +39-049 829 5083; fax: +39-049 870 0718.

E-mail address: zanca@igi.pd.cnr.it (P. Zanca).

0022-3115/01/$ - see front matter
PII: S0022-3115(00)00474-8

both fluid and Monte Carlo modelling [7], show that singly ionised carbon atoms should exist mainly in the first 2–3 cm layer close to the wall. Carbon influx is quite sensitive to the detail of the PWI, in that modifications of a few mm in the position of the last closed surface with respect to the wall may vary by some factors the brightness of the monitored emission line. On the other hand a correct determination of the influx requires the knowledge of both density and temperature of the local plasma, which is not a simple task. In any case CCD images are an excellent means to spatially identify regions of different PWI. Besides carbon emission, in the images one can easily recognise regions of bright emission that are to be identified mainly as high surface temperature spots ($T_s > 700$–$800°C$), which typically coincide with the edges of the graphite tiles or the protection caps of the clamping keys (hot spots in the middle of the tile).

3. Magnetic analysis

The analysis of the magnetic perturbation associated to the LM is based on the measurements of a system of external magnetic probes. Two poloidal arrays of radial field pick-up coils located on the inner surface of the shell ($r = b = 0.538m$) show that the poloidal harmonics content of the perturbation consists of at $m = 1$ mode plus a secondary $m = 0$ component. These perturbations correspond to a geometrical distortion of the plasma surface. The $m = 1$ kink is a radial displacement of the plasma surface centre characterised at any toroidal angle φ by the amplitude $\Delta(\varphi)$ and the poloidal direction $\Theta(\varphi)$. In [4] the solution of the vacuum Maxwell equations allow to derive generalised Shafranov formulas by which the $m = 1$ magnetic perturbation is correlated to the non-axisymmetric plasma surface displacement. Using these expressions and the measurements of two toroidal arrays of B_φ pick-up coils located at $r = b$, it is possible to estimate the quantities $\Delta(\varphi)$, $\Theta(\varphi)$ In Fig. 1(a) and (b) is shown the result for a particular shot. The plasma surface distortion follows an helical path whose amplitude is modulated by $\Delta(\varphi)$. The toroidal position of the LM is defined as the angle φ_{Lock} corresponding to the maximum of $\Delta(\varphi)$. The maximum value of $\Delta(\varphi)$ usually lies in the range 2–4 cm.

The $m = 0$ perturbation is instead a local variation of the plasma radius expressed by the bulging $\delta(\varphi)$. The toroidal flux measurements given by four loops arranged on the outer side of the vacuum vessel ($r = r_f = 0.5m$) show an $m = 0$ perturbation strictly correlated to the LM position. The bulging of the magnetic surfaces nearby $r = r_f$ can be simply related to the $m = 0$ flux [5] and it is extrapolated to the plasma radius by means of the toroidal field measurements mentioned above. Since on RFX the flux measurements are available only at

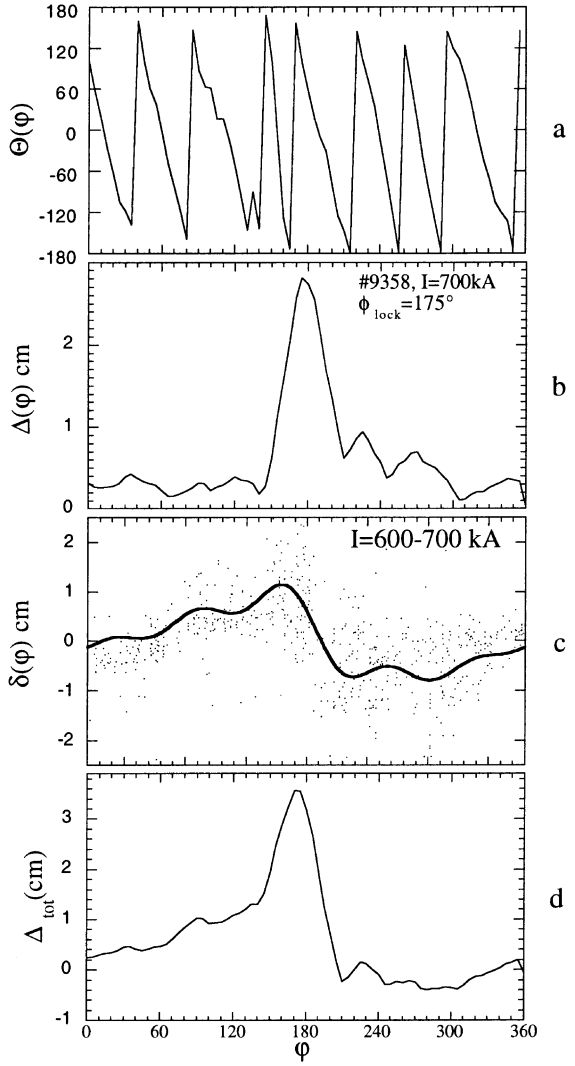

Fig. 1. Toroidal behaviour of the $m = 0, 1$ perturbation: (a) poloidal direction of the $m = 1$ kink; (b) amplitude of the $m = 1$ kink; (c) $m = 0$ bulging (the points are the data used for the ensemble average); (d) global displacement due to both the perturbations.

four toroidal positions, the shape of the perturbation cannot be reconstructed on a shot-by-shot basis, but only as an ensemble average over a large number of pulses with different φ_{Lock}. The typical profile thus obtained is shown in Fig. 1(c). This typical shape corresponds to a shrinking of the plasma minor radius in a position close to the maximum amplitude of the helical perturbation. The perturbation in Fig. 1(c) refers to shots with currents $600 < I < 700$ kA. Similar analysis made on different current intervals show that this $m = 0$ shape remains the same, whereas its amplitude strongly decreases with the plasma current: at intermediate and high currents it is much less relevant than the $m = 1$

kink, but at low current, say $I < 400$ kA , it becomes comparable.

4. Comparison with the CCD data

We assume that the intensity of the plasma–wall interaction is related to the radial displacement of the plasma surface contour from the axisymmetric equilibrium position. Combining both the $m = 0, 1$ perturbations, at a given position θ, φ this quantity is expressed by the function:

$$\delta r(\theta, \varphi) = \Delta(\varphi) \cdot \cos[\theta - \Theta(\varphi)] + \delta(\varphi). \quad (1)$$

The interaction should correspond only to outward displacements, i.e. to regions where $\delta r > 0$. The region of maximum interaction follows the helical path $\theta = \Theta(\varphi)$ and the corresponding displacement is $\Delta_{\text{tot}}(\varphi) = \Delta(\varphi) + \delta(\varphi)$. This quantity is reported in Fig. 1(d) for a shot with current $I \approx 700$ kA: the $m = 1$ shift Δ is computed for that particular discharge while the bulging is the typical profile for $600 < I < 700$ kA. The $m = 0$ contribution is expected to determine an asymmetry of the plasma–wall interaction with respect to the LM position, in particular to enhance the phenomenon for toroidal angles $\varphi < \varphi_{\text{Lock}}$.

We have compared the CCD images with the contour plots of the quantity δr for several discharges at different currents. In Figs. 2 and 3 two sample cases are shown with currents of 300 and 700 kA, respectively. A grid of poloidal and toroidal angles is superimposed to the images. The grid coincides with the edges of the graphite tiles. The contour plots are drawn in the (θ, φ) region seen by the CCD camera. The $m = 0$ profiles adopted in the formula (1) are the typical perturbations for those particular current values. The dashed lines superimposed both to the images and to the contour plots are portions of the curves $\theta = \Theta(\varphi)$. Both the images and the contour plots are averages in the time intervals specified in the captions.

From the CCD data two main features in the plasma–wall interaction emerge: the hot-spots on the tile edges, and the highly emissive diffuse halo. The hot-spots are present only in the high current shots and are connected to a strongly localised heat deposition. A good correspondence between the helical path of the perturbation and the position of the hot-spots is found. In particular the line of maximum magnetic perturbation separate the hot spots on the higher edges which are at higher φ from those on the lower edges which are at

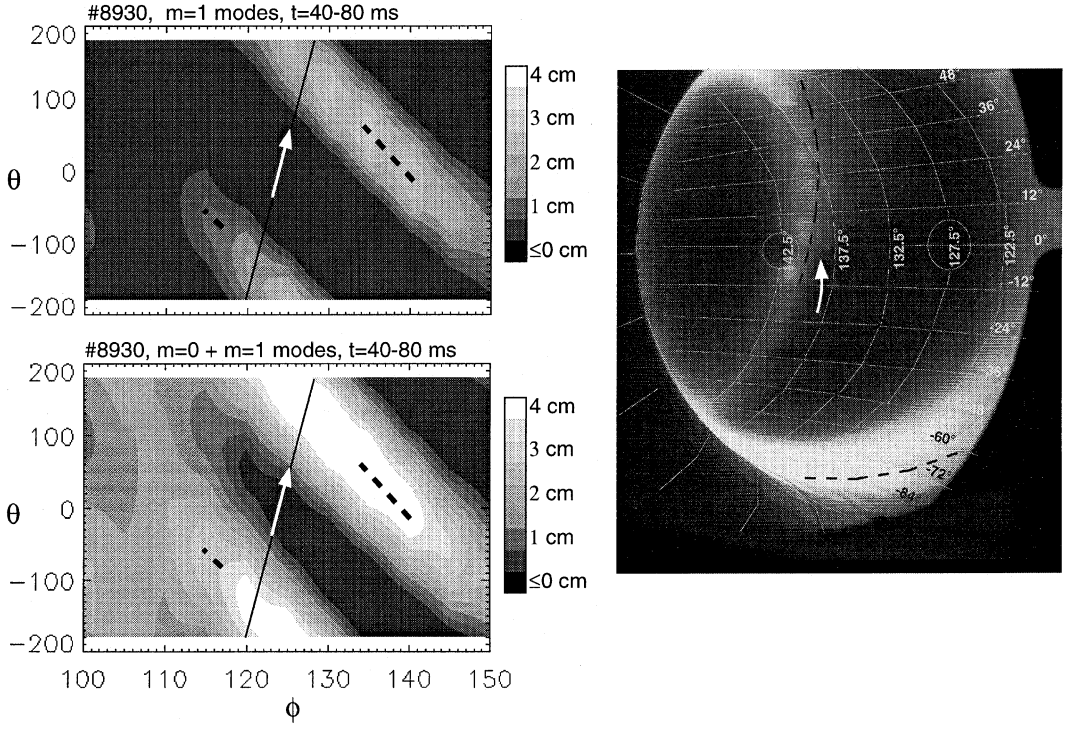

Fig. 2. Comparison between magnetic (at left) and CCD data (at right) for pulse #8930, $I = 300$ kA. Magnetic contour plots obtained with the $m = 1$ perturbation only (top) and with both the $m = 0, 1$ contributions (bottom) are shown. The dashed lines are portions of the curve $\theta = \Theta(\varphi)$. The arrows show the direction of the parallel electron drift along the magnetic field lines at the plasma edge.

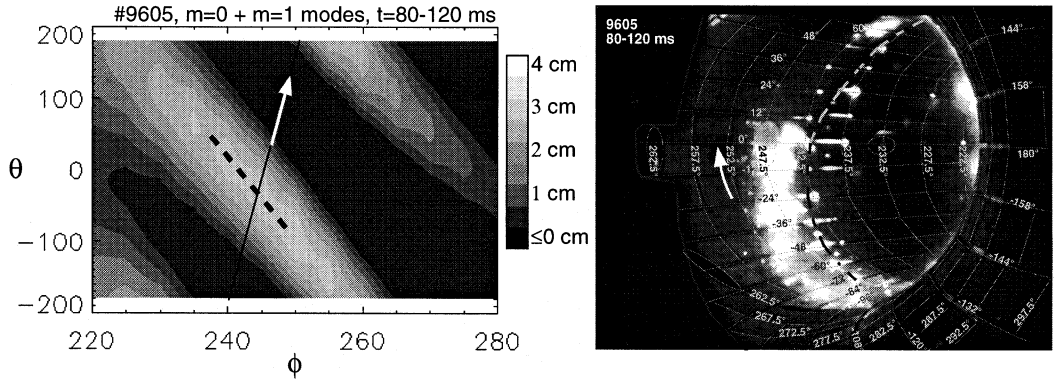

Fig. 3. Comparison between magnetic and CCD data for pulse #9605, $I = 700$ kA. The magnetic contour plot is obtained with both the perturbations $m = 0, 1$. The curve $\theta = \Theta(\varphi)$ matches the hot-spots positions, while the diffuse cloud is located at higher toroidal angles. The arrows show the direction of the parallel electron drift along the magnetic field lines at the plasma edge.

lower φ. This is consistent with the fact that they are produced by the parallel transport along the field lines that intersect the graphite wall. In fact the displacement of the plasma surface produces a limiter effect and the position of the hot-spots matches the pitch of the magnetic lines in the external region (which is opposite to the pitch of the perturbation).

The emission halo is visible both at low current (see Fig. 2) and, in many cases, at high current (Fig. 3). At low current the cloud is always present and has a quite regular shape, whereas at high current the cloud sometimes is not clearly visible and in general has a more irregular shape. A common feature observed in all the discharges is that this cloud is shifted at higher φ with respect to the maximum magnetic perturbation line. A similar asymmetry had been observed in the past when the LM had been compared with the measurements of a multichord interferometer [8] and of a tomographic bolometer [9]. In the former case a thin edge region of very high and highly fluctuating density had been identified. In the latter case the LM had been associated to a band of high edge radiation. It seems reasonable to assume that in all the above three cases the underlying phenomenon was the same: namely a cloud of high density plasma due to the enhanced influxes coming from The PWI region. The clouds seen by the CCD in particular are likely due to low ionisation carbon ions which are strongly emissive in the visible range.

As for the asymmetry relative to the LM path, a possible explanation could be the presence of the $m = 0$ magnetic perturbation which at angles $\varphi > \varphi_{\text{Lock}}$ determines a magnetic surfaces shrinking. In this way a scrape-off layer region is created, which can effectively collect the particle and power outflow pertaining to a significant part of the torus and concentrate it in a relatively narrow region close to the path of maximum magnetic perturbation. Conversely in the region $\varphi < \varphi_{\text{Lock}}$ the impact angle between the field lines and the tiles surfaces is lower: the plasma remains relatively close to the first wall and probably a true scrape-off layer cannot develop. The incident ion flux is spread over a much larger distance, which results in a lower sputtering yield, thus preventing the formation of the emissive cloud.

In the low current shot (Fig. 2) the brightest portion of the emission cloud is not centred with respect to the LM position, which is at $\varphi_{\text{Lock}} \approx 135°$. Indeed it is clear that a region of bright emission extends through all the inner poloidal section (hidden from the CCD view) which extends between $\varphi \approx \varphi_{\text{Lock}}$ and $\varphi \approx 122.5°$. This suggests the presence of a significant contribution due to the $m = 0$ bulging, as confirmed by comparing the contour plots with and without this component (Fig. 2). In fact the most intense region of emission fits quite well the contour of highest displacement with both the $m = 0$ and $m = 1$ contributions (bottom left Fig. 2), whereas it shows a worse agreement with the contour with the $m = 1$ contribution only (top left Fig. 2). Moreover, the ring-shaped region which can be seen at $\varphi = 120°$ finds a correspondence only in the contour plot with both the $m = 0$ and $m = 1$ contributions.

Concerning the $m = 0$ perturbation it is to be noticed that, although due to the ensemble average technique the profile of Fig. 1(c) had to be done with only the six lowest toroidal harmonics, there are other indications [5] that the $m = 0$ perturbation contains a larger harmonics spectra. The extra contribution should make the jump of the profile in correspondence of φ_{Lock} deeper and steeper, which would further improve the agreement between magnetic and CCD camera.

5. Summary and conclusions

The comparison between the CCD data on localised PWI and the non-axisymmetric magnetic perturbation of the plasma surface in RFX has on the one hand

confirmed the accuracy of the magnetic reconstruction method and, on the other hand, highlighted some important features of the PWI caused by locked mode.

The path of maximum radial displacement of the magnetic surface matches exactly the footprints of the 'hot spots' seen on the graphite tiles edges, which are due to the strongly localised power deposition associated to parallel heat flow along field lines directly striking the first wall. The agreement between CCD and magnetic data indicates that the spatial accuracy of the latter is of the order of a few cm.

For the first time, the contribution of that $m = 0$ components of the dynamo modes has been included in the magnetic analysis. Due to the lack of a suitable magnetic measurements, this has been done using a mean perturbation obtained by ensemble average over a large database. Nevertheless, the contribution of the $m = 0$ modes has been shown to be necessary in order to recover a good agreement between magnetic and CCD data, in particular for the low current pulses. This also confirms the different current scaling of the $m = 0$ and $m = 1$ perturbation amplitudes [5], i.e. the $m = 0$ perturbations are comparable to the $m = 1$ at low currents, whereas they become less important for plasma currents in the MA range.

Another feature of the localised PWI which emerged from the analysis is the presence of a highly emissive diffuse halo only on one side of the helical displacement of the magnetic surface. The asymmetry relative to the helical path of maximum radial displacement could be related to the asymmetric bulging due to the $m = 0$ modes.

References

[1] S. Ortolani, D.D. Snack, Magnetohydrodynamics of Plasma Relaxation, World Scientific, Singapore, 1993.
[2] R. Fitzpatrick, Phys. Plasmas 6 (1999) 1168.
[3] R. Bartiromo et al., Nucl. Fus. 39 (1999) 1697.
[4] P. Zanca, S. Martini, Plasma Phys. Control. Fus. 41 (1999) 1251.
[5] P. Zanca, S. Martini, Plasma Phys. Control. Fus. (2000), submitted.
[6] R. Pasqualotto et al., Plasma Dev. Ope. 5 (1998) 287.
[7] F. Sattin et al., in: Proceedings of 25th Conference on Plasma Physics and Controlled Fusion, vol. 22C, Prague, European Physical Society, 1998, p. 778.
[8] M. Valisa et al., J. Nucl. Mater. 241 (1997) 988.
[9] L. Marrelli, P. Zanca et al., J. Nucl. Mater. 266–269 (1999) 877.